




Modulation of Ion and Electron Pitch Angle in the Presence of Large-amplitude, Low-frequency, Left-hand Circularly Polarized Electromagnetic Waves Observed by *MMS*

J. S. Zhao^{1,2} , T. Y. Wang², M. W. Dunlop^{2,3}, J. S. He⁴, X. C. Dong³, D. J. Wu¹, Yu. V. Khotyaintsev⁵, R. E. Ergun⁶, C. T. Russell⁷, B. L. Giles⁸, R. B. Torbert⁹, and J. L. Burch¹⁰

¹ Key Laboratory of Planetary Sciences, Purple Mountain Observatory, Chinese Academy of Sciences, Nanjing 210008, People's Republic of China

² RAL Space, STFC, Oxfordshire, OX11 0QX, UK

³ School of Space and Environment, Beihang University, Beijing 100191, People's Republic of China

⁴ School of Earth and Space Sciences, Peking University, Beijing 100871, People's Republic of China

⁵ Swedish Institute of Space Physics, Uppsala SE-75121, Sweden

⁶ Laboratory of Atmospheric and Space Physics, University of Colorado, Boulder, Colorado 80303, USA

⁷ Institute of Geophysics and Planetary Physics, University of California, Los Angeles, CA, USA

⁸ NASA Goddard Space Flight Center, Greenbelt, MD 20771, USA

⁹ University of New Hampshire, Durham, New Hampshire, USA

¹⁰ Southwest Research Institute, San Antonio, Texas 78238, USA

Received 2018 July 26; revised 2018 August 24; accepted 2018 September 9; published 2018 October 30

Abstract

Most studies on low-frequency electromagnetic cyclotron waves have assumed a small wave amplitude, which ensures the reasonable application of linear and quasi-linear theories. However, the topic of large-amplitude electromagnetic cyclotron waves has not received much attention. Using *Magnetospheric Multiscale* measurements, this study observes low-frequency, left-hand circularly polarized electromagnetic waves with magnetic fluctuation $\sim 1\text{--}2$ nT in the dusk flank side of the Earth's magnetosheath. Considering the ambient magnetic field ~ 15 nT therein, the relative wave amplitude is of the order of 0.1. These large magnetic field fluctuations result in a periodic variation of the ion pitch angle. The electron pitch angle exhibits a localized distribution feature with a timescale approximating the wave period. Moreover, some electrons are trapped at a pitch angle $\sim 90^\circ$, and the trapping is more remarkable as strong waves arise. These two features of the electron pitch angle distribution imply that the trapping of electrons (partly) results from large-amplitude electromagnetic cyclotron fluctuations. Our results illustrate the important role of large-amplitude electromagnetic cyclotron waves on the dynamics of charged particles.

Key words: instabilities – plasmas – waves

1. Introduction

Low-frequency electromagnetic cyclotron waves (i.e., ion cyclotron waves) are usually observed in different solar-terrestrial environments, i.e., the Earth's magnetosphere, the magnetosheath, and the solar wind (e.g., Anderson & Fuselier 1993, 1994; Dunlop et al. 2002; Jian et al. 2014; Remya et al. 2014; Wicks et al. 2016; Zhao et al. 2018). These waves play an important role in the dynamics of charged particles. Linear and quasi-linear theories have shown that the resonance interaction of charged particles with ion cyclotron waves will result in the loss of relativistic electrons in the Earth's radiation belt (e.g., Summers & Thorne 2003; Summers et al. 2007; Jordanova et al. 2008) and the precipitation of ring current ions (e.g., Jordanova et al. 2001). Nonlinear mechanisms, including phase bunching and phase trapping of ions by ion cyclotron waves, can lead to a change in the ion pitch angle (e.g., Bortnik et al. 2010; Omidi et al. 2010; Zhu et al. 2012), i.e., the enhancement of low-energy protons and helium particles at the pitch angle $\sim 90^\circ$ observed by the *AST-6*, *GOES1* and 2, and *AMPTE/CCE* spacecraft (e.g., Mauk et al. 1981; Roux et al. 1982; Anderson & Fuselier 1994). However, in comparison with studies relating to small-amplitude waves, research on large-amplitude, low-frequency electromagnetic cyclotron waves has not attracted much attention.

Large-amplitude, circularly polarized electromagnetic proton cyclotron waves have been observed in the Earth's dusk-flank

magnetosheath by *Wind* and *Cassini* measurements (Tsurutani et al. 2002; Remya et al. 2014), which find the magnetic field fluctuation to be ~ 14 nT in the ambient magnetic field of ~ 55 nT. Using *Magnetospheric Multiscale* (*MMS*; Burch et al. 2016) measurements, this study provides other observational evidence for the existence of large-amplitude, low-frequency electromagnetic cyclotron waves in the dusk-flank side of the Earth's magnetosheath. We show that the wave amplitude is about 1–2 nT, where the ambient magnetic field is ~ 15 nT. The relative amplitude is of the order of 0.1. Since the plasma measurement in the *MMS* has high time resolution, i.e., 0.15 s for ions and 0.03 s for electrons, it provides an excellent opportunity to study ion and electron dynamics in the presence of large-amplitude electromagnetic waves.

Since we investigate both wave and particle behavior, we analyze *MMS* data from instruments including electric field double probes (Ergun et al. 2016; Lindqvist et al. 2016), fast plasma investigation (FPI; Pollock et al. 2016), and fluxgate magnetometers (Russell et al. 2016).

2. Observations

Figure 1 shows an overview of the observed wave during the time interval from 14:00:00 UT to 14:06:00 UT on 2017 October 7. The *MMS* is located at nearly $(-3.9, 23.7, 5.7)$ Earth radii in Geocentric Solar Magnetospheric coordinates, corresponding to the dusk-flank magnetosheath. The magnetic fluctuations are

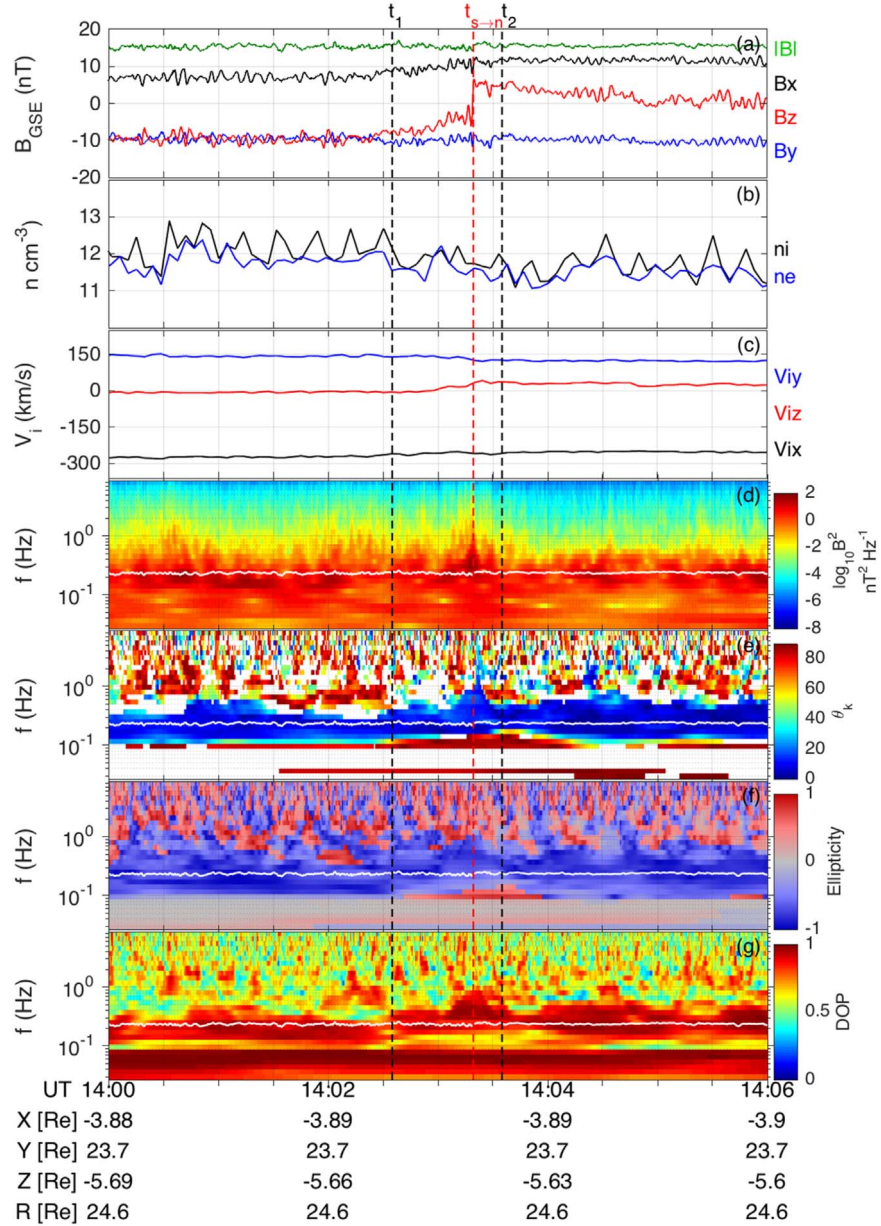


Figure 1. *MMS* overview of the low-frequency electromagnetic cyclotron wave from 14:00:00 to 14:06:00 UT on 2017 October 7. (a) Magnetic field in Geocentric Solar Ecliptic coordinates, (b) ion and electron density, (c) ion velocity, (d) power spectral density of the magnetic field, (e) wave normal angle, (f) wave ellipticity, and (g) degree of polarization. The solid lines in panels (d)–(g) denote the proton cyclotron frequency. $t_{s \rightarrow n}$ corresponds to the time when the direction of B_z changes from southward to northward. Brst data in the time interval $[t_1 t_2]$ is analyzed in Figures 3–4.

distinct over the whole time interval. At $t_{s \rightarrow n} \sim 14:03:37.37$ UT, which is denoted by the red vertical dashed line in Figure 1, the direction of B_z changes from southward to northward. The plasma density and ion streaming velocity are relatively steady. The averaged velocities, i.e., $V_{ix} \sim -265 \text{ km s}^{-1}$, $V_{iy} \sim 124 \text{ km s}^{-1}$, and $V_{iz} \sim 16 \text{ km s}^{-1}$, indicate ions streaming anti-parallel to the magnetic field. Polarization analysis in panels (d)–(g) show that the magnetic fluctuations in the frequency range $\sim [0.1, 0.5]$ Hz have the following properties: (1) degree of polarization larger than 0.8; (2) ellipticity smaller than -0.8 ; (3) the normal angle smaller than 20° or larger than 160° . A 180° uncertainty for the normal angle comes from the wavelet (Morlet) analysis used in panel (e). Because of the inverse Poynting flux (not shown in Figure 1), and the positive correlation between velocity and magnetic fluctuations (shown in Figure 2), we conclude the normal angle is larger than

160° . This wave information indicates that the mode corresponds to a nearly anti-parallel propagating, left-hand circularly polarized wave, usually called the electromagnetic ion cyclotron wave in studies of the planetary magnetosphere.

Figure 2 gives electromagnetic and velocity fluctuations in field-aligned coordinates. Since an abrupt change of the magnetic field configuration, not the wave fluctuation, occurs at nearly $t_{s \rightarrow n}$, we choose the time interval of 14:02:35.00UT–14:03:17.00UT before $t_{s \rightarrow n}$ to explore the general properties of the electromagnetic and velocity fluctuations. Full and filtered magnetic field components and velocity fluctuations are shown in panels (a) and (b). Referring to Figure 1, coherent waves concentrate in the frequency range $0.1 \text{ Hz} \leq f \leq 0.5 \text{ Hz}$; therefore, this frequency range is selected as the filtered frequency. The magnetic fluctuation is of the order of 1 nT, and the largest amplitude can

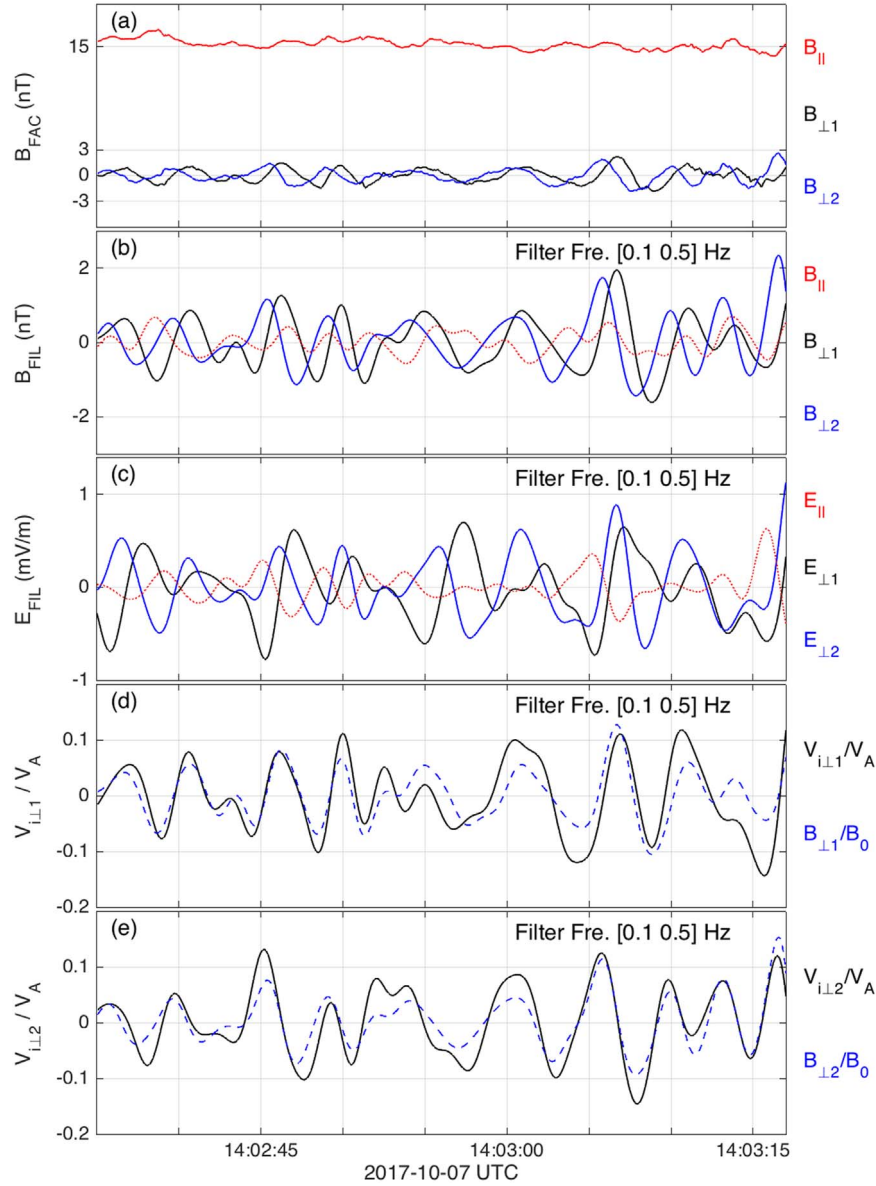


Figure 2. Electromagnetic and ion velocity fluctuations in magnetic field-aligned coordinates during 14:02:35.00UT–14:03:17.00UT. (a) Three magnetic field components, (b) magnetic fluctuations in the frequency range 0.1–0.5 Hz, (c) electric fluctuations in 0.1–0.5 Hz, (d), (e) ion velocities in units of Alfvén velocity in 0.1–0.5 Hz. The magnetic fluctuations are overlaid in panels (d)–(e), labeled by the dashed lines.

reach ~ 2 nT, where the ambient magnetic field is nearly 15 nT. The phase of $B_{\perp 1}$ is $\pi/2$ ahead of $B_{\perp 2}$, indicating the left-hand polarization mode. Also, left-hand polarization is seen from the phase relation between $E_{\perp 1}$ and $E_{\perp 2}$ shown in panel (c); the considerable B_{\parallel} and E_{\parallel} arise. Panels (d) and (e) present the phase relations between magnetic and velocity components, that is, $V_{i\perp}/V_A \simeq B_{\perp}/B_0$, indicating the wave propagating anti-parallel to the ambient magnetic field.

Figure 3 shows the ion energy distribution during the time interval from 14:02:35.00UT to 14:03:35.00UT. From panels (a), and (b), the ion omnidirectional flux mainly concentrates in the energy range $100 \text{ eV} \lesssim E_i \lesssim 1000 \text{ eV}$, and the ion pitch angle θ is normally larger than 90° . Panels (c)–(g) give the ion pitch angle distribution (IPD) in different energy ranges. A chaotic IPD appears in the low-energy range $2.16 \text{ eV} \leq E_i \leq 58.89 \text{ eV}$, indicating very low ion density therein. It is interesting to see a periodic variation of IPD in the energy ranges $77.98 \text{ eV} \leq E_i \leq 239.63 \text{ eV}$, $317.28 \text{ eV} \leq E_i \leq 736.45 \text{ eV}$, and

$975.08 \text{ eV} \leq E_i \leq 3967.62 \text{ eV}$. The change of pitch angle is nearly consistent with the variation of the angle $\theta_{B V_i}$ between the ion streaming velocity and magnetic field, defined as

$$\theta_{B V_i} = \arccos\left(\frac{\mathbf{B} \cdot \mathbf{V}_i}{|\mathbf{B}||\mathbf{V}_i|}\right).$$

Moreover, both θ and $\theta_{B V_i}$ variations are closely related to the magnetic fluctuations shown in panel (i). Therefore, Figure 3 provides observational evidence for modulation of the ion pitch angle by large-amplitude cyclotron waves. For high-energy ions, $5253.24 \text{ eV} \leq E_i \leq 28301.89 \text{ eV}$, there is no modulation feature in the IPD.

Figure 4 shows the electron energy distribution during the time interval from 14:02:35.00UT to 14:03:35.00UT. From the omnidirectional electron differential energy flux (panel (a)), the electron energy is normally smaller than 1 keV. The electron pitch angle distribution (EPD) in panels (b)–(h) exhibits different

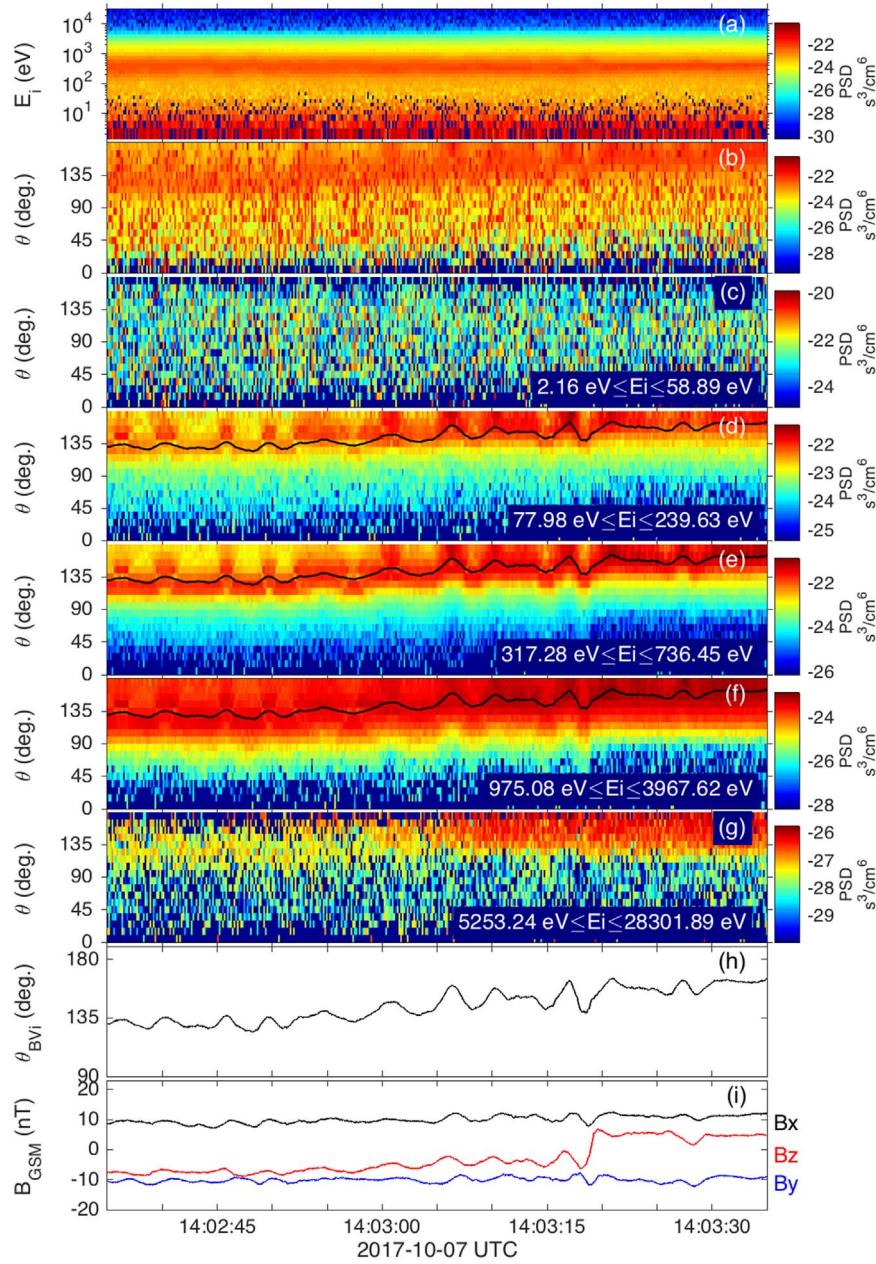


Figure 3. Ion dynamics in the time interval from 14:02:35.00UT to 14:03:35.00UT. (a) Omnidirectional ion differential energy flux, (b) ion pitch angle distribution (IPD) in the full energy range 2.16–28301.89 eV, (c)–(g) IPD in different energy ranges, (h) the angle θ_{BVi} between the ion streaming velocity and magnetic field, and (i) magnetic field in Geocentric Solar Magnetospheric coordinates. θ_{BVi} is overlaid in panels (d)–(f), labeled by black solid lines.

dynamics behaviors of electrons with different energy. For low-energy electrons, $6.52 \text{ eV} \leq E_e \leq 19.15 \text{ eV}$, the pitch angle θ is always larger than 135° before $t_{s \rightarrow n}$, and larger than 90° after $t_{s \rightarrow n}$. This indicates low-energy electrons mainly streaming anti-parallel to the magnetic field. In the energy range $25.07 \text{ eV} \leq E_e \leq 42.95 \text{ eV}$, most electrons move along the magnetic field, i.e., $\theta \lesssim 45^\circ$. We also find the appearance of cooling for electrons at $\theta_p < \theta < 180 - \theta_p$, where the critical pitch angle θ_p is defined as $\theta_p = \arcsin \sqrt{B/B_{\max}}$, B is the magnitude of the magnetic field, and B_{\max} is the maximal B during 14:02:35.00UT–14:03:35.00UT. Moreover, the cooling of trapped electrons arises in panel (e) where $56.23 \text{ eV} \leq E_e \leq 73.60 \text{ eV}$. For $E_e \gtrsim 216.11 \text{ eV}$, trapped electrons are slightly heating, shown in panels (g) and (h). On the other

hand, there exist many localized EPDs for electrons with $56.23 \text{ eV} \lesssim E_e \lesssim 830.63 \text{ eV}$. An example of localized EPD is shown as the band between the two vertical dashed lines in panels (e)–(g). The timescale of these localized EPDs approximates the period of the observed wave, implying the role of the large-amplitude cyclotron wave on the emergence of these confined electrons.

3. Discussion and Summary

Since the ion cyclotron anisotropic instability is widely believed to be the source of ion cyclotron waves in the Earth's magnetosphere (i.e., Cornwall 1965; Kennel & Petschek 1966), here we check the possibility of local excitation of the observed

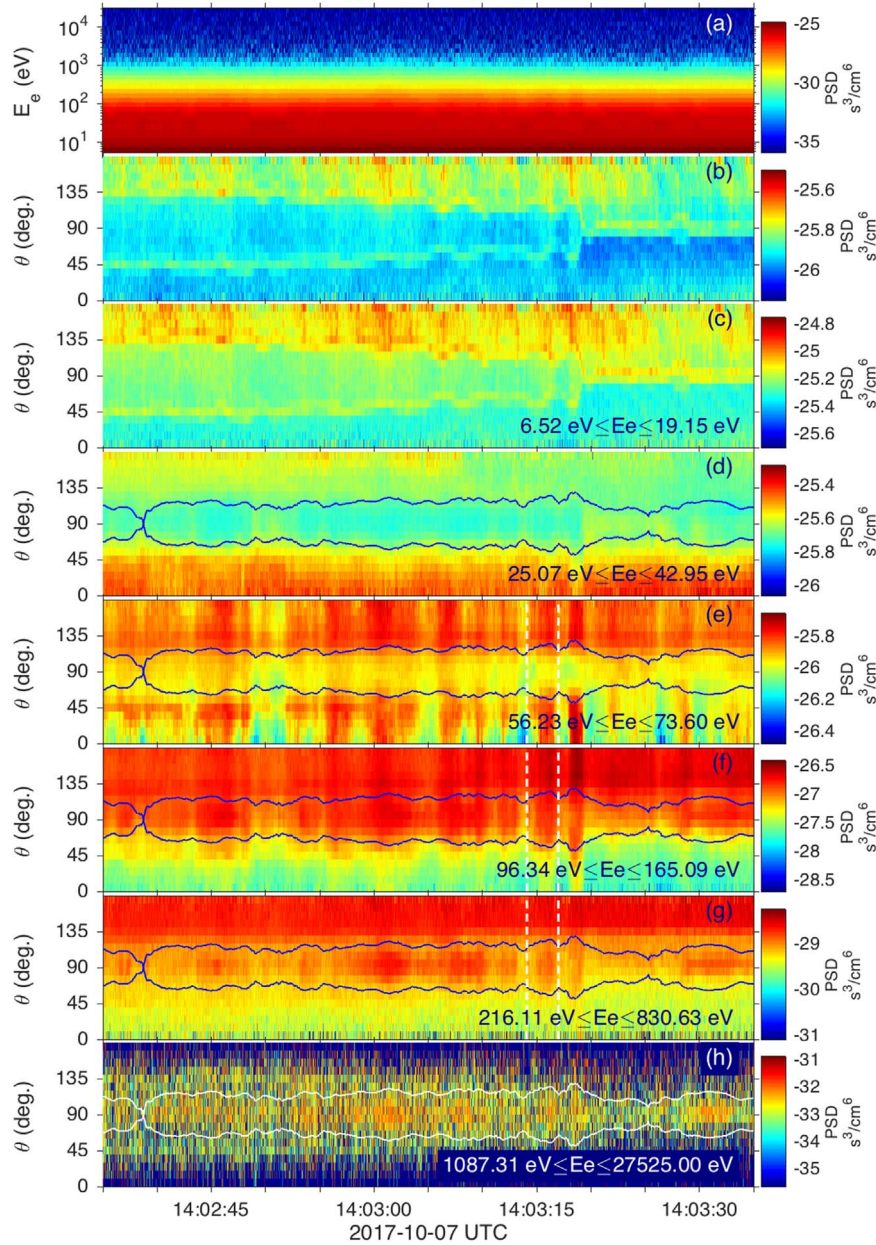


Figure 4. Electron dynamics during the time interval from 14:02:35.00UT to 14:03:35.00UT. (a) Omnidirectional electron differential energy flux, (b) electron pitch angle distribution (EPD) in the full energy range 6.52–27525.00 eV, and (c)–(h) EPD in different energy ranges. The solid lines overlaid in panels (d)–(h) represent critical pitch angles θ_p and $180^\circ - \theta_p$. An example of a localized EPD is shown as the band limited by the two vertical dashed lines in panels (e)–(g).

waves by this kind of instability. We adopt an instability threshold condition $(T_{i\perp}/T_{i\parallel} - 1) = 0.35/\beta_{\parallel}^{0.42}$ (corresponding to $\gamma/\Omega_{ci} = 10^{-4}$), assumed in plasmas only having electron and ion components (Gary & Lee 1994). Using the plasma parameters averaged from FPI during 14:02:35UT–14:03:17UT, $n_i = 12 \text{ cm}^{-3}$, $T_{i\parallel} = 91 \text{ eV}$, $T_{i\perp} = 111 \text{ eV}$, $T_{e\parallel} = 32 \text{ eV}$, $T_{e\perp} = 34 \text{ eV}$, and $B_0 = 15 \text{ nT}$, we find that $(T_{i\perp}/T_{i\parallel} - 1) = 0.22 < 0.35/\beta_{\parallel}^{0.42} = 0.27$. Therefore, there is no ion temperature anisotropy instability in our event. Also, we use WHAMP (a dispersion equation solver based on linear plasma kinetic theory, Rönnmark 1982), and find that the wave is damping, i.e., $\gamma \sim -0.003\Omega_{ci}$ at $\omega \sim 0.2\Omega_{ci}$. On the other hand, Narita et al. (2004) found that some of the low-frequency, left-hand-polarized Alfvén waves in the Earth’s foreshock propagate

downstream. Therefore, our observed waves may be generated nonlocally in the foreshock.

Since the observed waves propagate at $|\theta| \sim 0^\circ$, the wave frequency at the plasma frame is $\omega_{\text{plasma}}/\Omega_{ci} \approx (\omega_{\text{obs}}/\Omega_{ci})(1 + V_{\parallel}/V_A)^{-1} \approx 0.15 - 0.6$, where the parallel ion streaming velocity is $V_{\parallel} \approx 219 \text{ km s}^{-1}$, the Alfvén velocity is $V_A \approx 97 \text{ km s}^{-1}$ during 14:02:35UT–14:03:17UT, and the observed wave frequency is $\omega_{\text{obs}} \sim 0.5\Omega_{ci} - 2\Omega_{ci}$. From linear plasma theory we have linear responses among perpendicular electromagnetic components for the left-hand polarized cyclotron wave: $E_{\perp 2} = -iE_{\perp 1}$, $B_{\perp 2} = -iB_{\perp 1} = (k_{\parallel}/\omega)E_{\perp 1}$, and $V_{i\perp 2} = -iV_{i\perp 1} = -(\omega/k_{\parallel})(B_{\perp 2}/B_0)/(1 - \omega/\Omega_{ci})$ (i.e., Zhao 2015). When the wave is propagating anti-parallel to the ambient magnetic field, i.e., k_{\parallel} is negative, $E_{\perp 1}$ and $B_{\perp 2}$ are out

of phase, $E_{\perp 2}$ and $B_{\perp 1}$ are in phase, and $V_{i\perp 1,2}$ and $B_{\perp 1,2}$ are in phase. These theoretical predictions are consistent with our observations. Furthermore, when the wave is obliquely propagating, even at a small normal angle, the parallel electromagnetic fields E_{\parallel} and B_{\parallel} will arise; for example, $E_{\parallel} \sim 0.015E_{\perp 1}$ and $B_{\parallel} \sim 0.16B_{\perp 2}$ at $\omega \sim 0.2\Omega_{ci}$ as $|\theta| = 10^\circ$. Since the observed E_{\parallel} and B_{\parallel} , i.e., $E_{\parallel} \sim 0.2E_{\perp}$ and $B_{\parallel} \sim 0.5B_{\perp}$, are stronger than corresponding linear responses, this is in favor of E_{\parallel} and B_{\parallel} produced through the nonlinear mechanisms.

The most interesting finding in the study is the modulation of the ion and electron pitch angles by the observed large-amplitude electromagnetic cyclotron waves. The periodic variation of the pitch angle arises for ions with energy from $E_i = 77.98$ eV to $E_i = 3967.62$ eV. When ions stream into the dusk-flank side of the magnetosheath, owing to large magnetic fluctuations, they induce a variation of the angle between the ion streaming velocity and the magnetic field, which results in the ion pitch angle having a periodic variation. On the other hand, some electrons will be trapped in the inhomogeneous magnetic field due to large magnetic fluctuations. Cooling occurs for trapped electrons with 25.07 eV $\lesssim E_e \lesssim 73.60$ eV, and heating appears for trapped electrons with $E_e \gtrsim 216.11$ eV. Moreover, for electrons having 56.23 eV $\lesssim E_e \lesssim 830.63$ eV, their pitch angles exhibit an intermittent distribution feature, and the timescale is nearly the same as the wave period. This implies that electrons may be trapped by the large parallel electric field fluctuations. Therefore, the observed large-amplitude electromagnetic wave can affect both the dynamics of ions and electrons.

In summary, using *MMS*, this study observes the periodic variation of ion and electron pitch angles in the presence of large-amplitude, low-frequency, left-hand circularly polarized electromagnetic waves in the Earth's dusk-flank magnetosheath. Modulation of the ion pitch angle results from the change in the ion streaming velocity relative to the magnetic field including the ambient and fluctuation fields. Modulation of the electron pitch angle is induced by the inhomogeneous magnetic field structure, which is partly caused by the magnetic field fluctuation, and also probably by electrons trapped in the electromagnetic field of the large-amplitude wave.

This work was supported by the NNSFC 11673069, 41531071, by NSF of Jiangsu Province under grant No. BK20161617, and the Youth Innovation Promotion Association CAS. M.W.D. is supported by NNSFC 41874193 and 41574155, NERC grant NE/H004076/1, and by STFC in-house research grant. T.Y.W. is supported by the Marie Skłodowska-Curie grant No. 665593 from the European Union's Horizon 2020 research and innovation programme. J.S.H. is supported by NNSFC 41574168 and 41874200. The data are available from the *MMS* Science Data Center (<https://lasp.colorado.edu/mms/sdc/public/>).

ORCID iDs

J. S. Zhao  <https://orcid.org/0000-0002-3859-6394>

References

- Anderson, B. J., & Fuselier, S. A. 1993, *JGR*, **98**, 1461
 Anderson, B. J., & Fuselier, S. A. 1994, *JGR*, **99**, 19413
 Bortnik, J., Thorne, R. M., & Omid, N. 2010, *JGR*, **115**, A12242
 Burch, J. L., Moore, T. E., Torbert, R. B., & Giles, B. L. 2016, *SSRv*, **199**, 5
 Cornwall, J. M. 1965, *JGR*, **70**, 61
 Dunlop, M. W., Lucek, E. A., Kistler, L. M., et al. 2002, *JGRA*, **107**, 1228
 Ergun, R. E., Tucker, S., Westfall, J., et al. 2016, *SSRv*, **199**, 167
 Gary, S. P., & Lee, M. A. 1994, *JGR*, **99**, 11297
 Jian, L. K., Wei, H. Y., Russell, C. T., et al. 2014, *ApJ*, **786**, 123
 Jordanova, V. K., Albert, J., & Miyoshi, Y. 2008, *JGRA*, **113**, A00A10
 Jordanova, V. K., Farrugia, C. J., Thorne, R. M., et al. 2001, *JGR*, **106**, 7
 Kennel, C. F., & Petschek, H. E. 1966, *JGR*, **71**, 1
 Lindqvist, P.-A., Olsson, G., Torbert, R. B., et al. 2016, *SSRv*, **199**, 137
 Mauk, B. H., McIlwain, C. E., & McPherron, R. L. 1981, *GeoRL*, **8**, 103
 Narita, Y., Glassmeier, K.-H., Schäfer, S., et al. 2004, *AnGeo*, **22**, 2315
 Omid, N., Thorne, R. M., & Bortnik, J. 2010, *JGR*, **115**, A12241
 Pollock, C. J., Moore, T., Jacques, A., et al. 2016, *SSRv*, **199**, 331
 Remya, B., Tsurutani, B. T., Reddy, R. V., et al. 2014, *ApJ*, **793**, 6
 Rönmark, K. 1982, WHAMP—Waves in Homogeneous, Anisotropic, Multicomponent Plasmas, Tech. Rep. 179, Kiruna Geophysical Institute
 Roux, A., Perraut, S., Rauch, J. L., et al. 1982, *JGR*, **87**, 8174
 Russell, C. T., Anderson, B. R., Baumjohann, W., et al. 2016, *SSRv*, **199**, 189
 Summers, D., Ni, B., & Meredith, N. P. 2007, *JGRA*, **112**, A04206
 Summers, D., & Thorne, R. M. 2003, *JGRA*, **108**, 1143
 Tsurutani, B. T., Arballo, J. K., Zhou, X.-Y., Galvan, C., & Chao, J. K. 2002, in *COSPAR Coll. Ser., Space Weather Study Using Multipoint Techniques*, ed. L.-H. Lyu (Oxford: Pergamon Press), 97
 Wicks, R. T., Alexander, R. L., Stevens, M., et al. 2016, *ApJ*, **819**, 6
 Zhao, G. Q., Feng, H. Q., Wu, D. J., et al. 2018, *JGRA*, **123**, 1715
 Zhao, J. 2015, *PhPI*, **22**, 042115
 Zhu, H., Su, Z., Xiao, F., et al. 2012, *JGR*, **117**, A12217